JACS
JOURNAL OF THE AMERICAN CHEMICAL SOCIETY
Communication
pubs.acs.org/JACS

New Two-Dimensional Niobium and Vanadium Carbides as Promising Materials for Li-Ion Batteries

Michael Naguib,[†,‡] Joseph Halim,[†,‡,§] Jun Lu,[§] Kevin M. Cook,[†,‡] Lars Hultman,[§] Yury Gogotsi,*[,†,‡] and Michel W. Barsoum*[,†]

[†]Department of Materials Science & Engineering, Drexel University, Philadelphia, Pennsylvania 19104, United States
[‡]A.J. Drexel Nanotechnology Institute, Drexel University, Philadelphia, Pennsylvania 19104, United States
[§]Thin Film Physics Division, Department of Physics (IFM), Linköping University, S-581 83 Linköping, Sweden

Supporting Information

ABSTRACT: New two-dimensional niobium and vanadium carbides have been synthesized by selective etching, at room temperature, of Al from Nb_2AlC and V_2AlC, respectively. These new matrials are promising electrode materials for Li-ion batteries, demonstrating good capability to handle high charge−discharge rates. Reversible capacities of 170 and 260 mA·h·g^{-1} at 1 C, and 110 and 125 mA·h·g^{-1} at 10 C were obtained for Nb_2C and V_2C-based electrodes, respectively.

Two-dimensional (2D) materials have garnered great attention during the past decade. Interest was further enhanced after the discovery of graphene's unique electronic properties by Novoselov et al.[1] Other 2D materials, such as boron nitride,[2] as well as transition metal chalcogenides,[3] metal oxides, and hydroxides have also been thoroughly explored.[4] Recently, our discovery of 2D early transition metal carbides and carbonitrides that we labeled *MXenes* further extended the family of 2D inorganic materials to include: Ti_3C_2, Ti_2C, Ta_4C_3, $(Ti_{0.5},Nb_{0.5})_2C$, $(V_{0.5},Cr_{0.5})_3C_2$, and Ti_3CN.[5a,b] MXenes are produced by selectively etching the "*A*" metal from *MAX* phases, a family of 60+ hexagonal, machinable early transition metal, layered ternary carbides and/or nitrides with a general formula $M_{n+1}AX_n$ (bottom inset in Figure 1a). In the MAX phases, *M* is an early transition metal, *A* represents a group A (mostly groups 13 and 14) element, *X* represents C and/or N, and n = 1, 2, or 3.[6] The etching was carried out by soaking $M_{n+1}AlX_n$ powders in aqueous hydrofluoric acid (HF) at room temperature (RT). The HF selectively etches out the Al, which, in turn, is replaced by OH, O, and/or F. The replacement of strong metallic bonds between the M−A layers by weaker hydrogen bonds allows for the facile separation of 2D MXene layers with the aid of sonication.[5a,b] To differentiate surface terminated MXenes from bare surfaces, we henceforth will refer to them as $M_{n+1}X_nT_x$

Density functional theory (DFT) calculations, which were conducted for a much larger number of MXene structures, show that their electronic structure depends on their surface termination. Bare MXenes surfaces are predicted to be metallic conductors, whereas MXenes with OH, O, or F are predicted to be semiconductors, but with band gaps ranges from 0.05 to 1.8 eV.[5b,7a,b] Some MXenes are expected to be excellent thermoelectric materials.[7b] Ab initio calculations also predict that

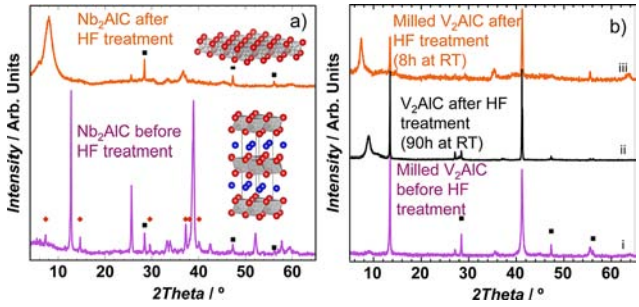

Figure 1. XRD diffraction patterns for (a) Nb_2AlC before and after HF treatment. The black squares represent peaks belonging to Si added as an internal reference. The peaks denoted by the red diamonds represent Nb_4AlC_3 peaks that existed in the Nb_2AlC sample as a secondary phase before HF treatment. The structures shown in inset represent, from bottom to top, the M_2AX and M_2X structures, respectively (M atoms are shown in red and A in blue). (b) V_2AlC before and after HF treatment. In all cases, the samples were cold pressed to 450 MPa to highly orient the basal planes and enhance their signal.

MXenes should possess high elastic moduli when pulled along their basal planes.[8]

Potential applications for MXenes range from conductive reinforcement fillers for polymers,[9] to catalysts and sensors, transparent conductors, and many others. Of special interest to this work is the use of MXenes as electrode materials in electrical energy storage such as supecapacitors,[10] lithium ion batteries (LIBs),[11a−c] and lithium ion capacitors.[12] The lithiation and delithiation mechanisms were found to be Li intercalation and deintercalation between the MXene layers.[12] In general, MXenes with n = 1, viz., M_2X (top inset in Figure 1a), should have higher gravimetric capacities compared to their higher order counterparts such as M_3X_2[11c] or M_4X_3, because the former have less atomic layers compared to the latter (3 atomic layers vs 5 and 7, respectively). Furthermore, M_2X-based MXenes should possess higher specific surface areas as compared to their higher order counterparts.

Herein we report, for the first time, on the synthesis of two new 2D phases, Nb_2CT_x and V_2CT_x, and their Li uptake and cyclability at high rates. The 2D Nb_2CT_x material was synthesized by treating Nb_2AlC (synthesis protocols and

Received: June 7, 2013
Published: October 8, 2013

   dx.doi.org/10.1021/ja405735d | *J. Am. Chem. Soc.* 2013, 135, 15966−15969

characterization techniques are described in the Supporting Information, SI) in aqueous HF (50% conc. at RT for 90 h). X-ray diffraction (XRD) patterns (Figure 1a) show that the 100% intensity diffraction peak, around 2θ of 38.9°, for Nb_2AlC vanishes after treatment. More importantly, the (0002) peak broadens and downshifts significantly to an angle corresponding to a *c* lattice parameter, *c*-LP, of 22.34 Å, instead of 13.88 Å for pristine Nb_2AlC. The total disappearance of the (0002) peak associated with the latter implies that the entire sample was converted to MXene. Similar shifts were observed for other MXenes.[5a,b] From the broadening of the (0002) peak and using Scherrer's equation,[13] the domain size along [0001] is estimated to be ≈5 nm. The yield, defined here as the weight of powder after HF treatment/weight of the pristine powder × 100, was around 100%. Note that as defined here the yield is a convoluted function of fraction of unreacted and dissolved MAX phase, as well as the extent to which the layers are hydrated or terminated (see below).

To shed more light on the reaction and surface terminations, the compounds were analyzed by energy-dispersive X-ray spectroscopy (EDS) and X-ray photoelectron spectroscopy (XPS). The Nb:C:O:F:Al atomic ratios determined by EDS, normalized to those of Nb, were found to be around 2.00:1.59(±0.05):2.79(±0.14):0.99(±0.04):0.08(±0.01). Since no Nb_2AlC peaks were observed in the XRD patterns, it is reasonable to assume that all remaining Al in the etched powders is in the form of aluminum fluoride salts. In general, estimating the C content from EDS spectra is problematic since C is readily found as a contaminant. The problem is exacerbated in Nb-containing materials because the K_α energy of C and the M_{IV} energy of Nb are close to each other in energy. Given that there is no external source for C in the etching process that could increase the C content in the material, we henceforth assume that the Nb:C ratio is 2:1 instead of the 2:1.6 measured in EDS. In this case, the Nb:C ratio in Nb_2AlT_x remains 2:1 and our conclusion concerning the MXene chemistry does not change. For the same reason, the V:C ratio is assumed to be 2:1. High-resolution XPS spectra in the Nb, C, and O regions indicated the presence of Nb_2C MXene layers terminated in a mixed oxide/fluoride layer, as well as the presence of physisorbed water (Figure S1). The high oxygen content measured by EDS could thus be due to water intercalated between the MXene layers, which would be difficult to remove completely.

A small amount of Nb_4AlC_3 existed as a secondary phase in the starting Nb_2AlC sample (Figure 1a). The latter was also fully converted into MXene after treatment as evidenced by XPS (see SI). Its *c*-LP increased from 24.19 to ≈30.47 Å. This implies that it should be straightforward to produce 2D sheets of Nb_4C_3 (synthesis of this MXene structure has not yet been reported). Note that the presence of Nb_4C_3 may be partially responsible for the C content being higher than stoichiometric for Nb_2C.

In case of V_2C, the yield after HF (50% conc.) treatment at RT for 90 h was around 60%. Post HF treatment XRD patterns (Figure 1bii) show some unreacted V_2AlC, together with a new broad peak around 2θ of 8.96°. This peak can be assigned to the (0002) plane of MXene, and translates to a *c*-LP of 19.73 Å. We note in passing that using the 0002 peak line intensities to quantify the amount of unreacted V_2AlC is somewhat problematic because the V_2C powders are much less ordered than the parent material, producing weaker and broadened diffraction lines. So, it is more accurate to use the EDS to estimate the amount of unreacted MAX phase. For example, in the aforementioned sample, the V:Al ratio was >2.0:0.2, implying that more than 80% of the V_2AlC was converted into V_2C. The unreacted V_2AlC was conjectured to result from the presence of some large V_2AlC particles in the starting powder. Recently we have shown that a powder particles' size plays an important role in the rate at which Ti_3AlC_2 converts to Ti_3C_2.[14]

To test this idea, V_2AlC powders were attrition milled prior to their immersion in the HF (50% conc.) solutions at RT for 8 h. The yield was ∼55%. The XRD pattern (Figure 1biii) showed evidence for both unreacted V_2AlC and V_2C. The *c*-LP of the latter, at 23.96 Å, was significantly larger than that of V_2C produced from unmilled V_2AlC after 90 h in HF. The reason for this is most likely the presence of water or reaction products between the MXene layers, which should occur more readily for sheets of smaller lateral dimensions. Its exact origin, however, is a topic of ongoing research. The results suggest, however, that it may be possible to tune the *c*-LP of V_2CT_x by controlling the etching and initial particle size parameters. Attrition milling did not enhance the overall yield, but reduced the etching time from 90 h to 8 h.

It is important to note that the expansions in the *c*-LPs for V_2CT_x and Nb_2CT_x compared to their parent MAX phases are significantly larger than the expansion of Ti_2CT_x relative to its parent phase. Here again the exact reason is unclear, but the large expansions suggest that significantly more water intercalates between the V_2CT_x and Nb_2CT_x layers than between Ti_2CT_x. It is crucial to note here that without assuming that H_2O molecules are intercalated in between the MXene layers, it is difficult to rationalize the large *c*-LPs observed (22−24 Å). Spontaneous water intercalation has been reported for other layered materials.[15] Needless to add, cointercalation of reaction products is also possible.

The EDS results of V_2AlC after the RT 8 h HF treatment indicated the presence of V, C, O, F, and small amounts of Al in an atomic ratio of 2.00:1.01(±0.11):1.35(±0.07):1.06(±0.07):0.14(±0.01), respectively. Assuming conservatively, that the entirety of the Al signal originates from unreacted V_2AlC, the amount of the latter would be around 15 wt % after treatment. On the basis of that assumption, the V:C:O:F in MXene would be ≈2:1:1.5:1.2, respectively. However, since some Al may also exist in the form of aluminum fluoride salts[5b] that had not been completely washed from the MXene powders, it is reasonable to assume the amount of unreacted V_2AlC to be less than 15 wt%. Additionally, high-resolution XPS spectra in the V, C, and O regions indicated the presence of V_2CT_x layers terminated in a mixed oxide/fluoride layer, together again with the presence of physisorbed water (Figure S2).

On the basis of the XRD, XPS, and EDS results, we conclude that the following simplified reactions:

$$Nb_2AlC + 3HF \rightarrow Nb_2C + AlF_3 + 1.5H_2\uparrow \quad (1)$$

$$V_2AlC + 3HF \rightarrow V_2C + AlF_3 + 1.5H_2\uparrow \quad (2)$$

followed by surface reactions of the transition metal atoms with solution species that in turn lead to the O, OH, and F terminations described in our previous work.[5a,b]

Scanning electron microscope (SEM) images of Nb_2CT_x and V_2CT_x powders shown in Figure 2, panels a and b, respectively, exhibit the typical layered morphology of MXenes.[5a,b] As noted previously, such morphologies are reminiscent of exfoliated graphite.[16] The same is true of transmission electron microscope (TEM) images for both Nb_2CT_x (Figure 2c) and V_2CT_x (Figure 2e). Selected area electron diffraction (SAED) for Nb_2CT_x (inset Figure 2c) shows that the hexagonal basal structure of the parent

dx.doi.org/10.1021/ja405735d | J. Am. Chem. Soc. 2013, 135, 15966−15969

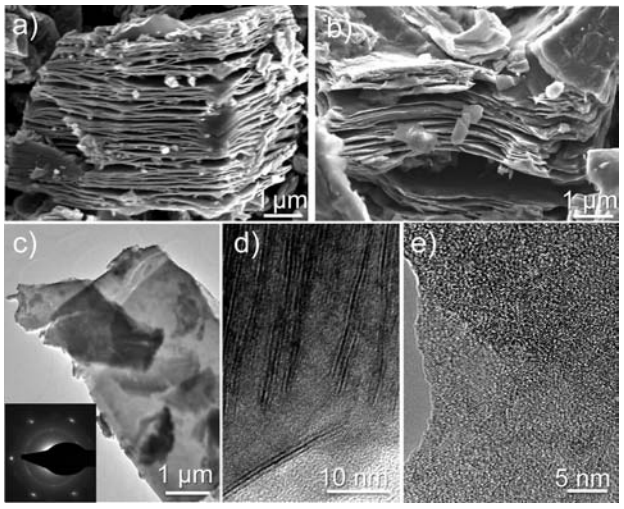

Figure 2. Electron microscope images of HF treated powders: (a and b) SEM images of Nb_2CT_x and V_2CT_x powders, respectively; (c) TEM image of Nb_2CT_x flake. Inset represents the SAED showing the hexagonal basal plane symmetry, which is identical to that of the parent MAX phase. (d) Cross section TEM image of Nb_2CT_x and (e) in-plane TEM image of a V_2CT_x flake.

MAX phase is preserved after HF treatment. When the basal planes are observed in cross section in a TEM image (Figure 2d), it is clear that some MXene flakes are ~1 nm thick, viz., 2 M_2X layers thick. Furthermore, $Nb_4C_3T_x$ layers were observed in TEM cross-sectional micrographs (Figure S3). The *d* spacing measured from the corresponding SAED was in good agreement with the values calculated from XRD. Figure 2e shows a typical TEM micrograph of V_2CT_x, from which it is reasonable to conclude that the number of MXene layers is small.

To explore the feasibility of using Nb_2CT_x and V_2CT_x as electrodes in LIBs, cyclic voltammetry (CV) and galvanostatic charge−discharge cycling (GV) were carried out. The CV curves for Nb_2CT_x (Figure S4a) showed no significant lithiation and delithiation capacity at voltages higher than 2.5 V. Hence, the GV for Nb_2CT_x was carried out between 0 and 2.5 V against Li/Li^+. The voltage profile for Nb_2CT_x at 1 C cycling rate (Figure 3a)

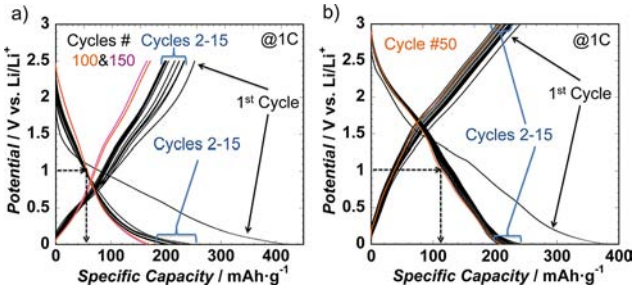

Figure 3. Electrochemical performance of Nb_2CT_x and V_2CT_x as electrodes in LIB. (a) Voltage profile of Nb_2CT_x between 0 and 2.5 V vs Li/Li^+. (b) Voltage profile of V_2CT_x (produced by HF treatment of V_2AlC at RT for 90 h) between 0 and 3 V vs Li/Li^+.

yields a first cycle capacity of ~422 $mA{\cdot}h{\cdot}g^{-1}$. The second cycle capacity was about 250 $mA{\cdot}h{\cdot}g^{-1}$. The reason for the first cycle irreversibility could be due to solid electrolyte interphase (SEI) formation or due to irreversible reaction of Li with the surface groups and/or water molecules in the as-synthesized MXene. In principle, this irreversibility could be minimized by controlling the surface chemistry of MXene or by prelithiating the electrode material as reported for other systems.[17] After 100 cycles, a reversible capacity of 170 $mA{\cdot}h{\cdot}g^{-1}$ was obtained. And while 170 $mA{\cdot}h{\cdot}g^{-1}$ is comparable to what was reported for hollow nanospheres of niobium oxide,[18] the average lithiation voltage is lower in our material.

Because the CV for V_2CT_x (Figure S4b) showed a large capacity close to 3 V, this material was tested between 0 and 3 V against Li/Li^+. Figure 3b shows the voltage profile at 1 C. The first cycle capacity was found to be ~380 $mA{\cdot}h{\cdot}g^{-1}$ and the reversible capacity ~210 $mA{\cdot}h{\cdot}g^{-1}$. Intriguingly, the V_2CT_x, produced by etching attrition milled V_2AlC, showed >30% enhancement in Li uptake (Figure 4) compared to V_2CT_x

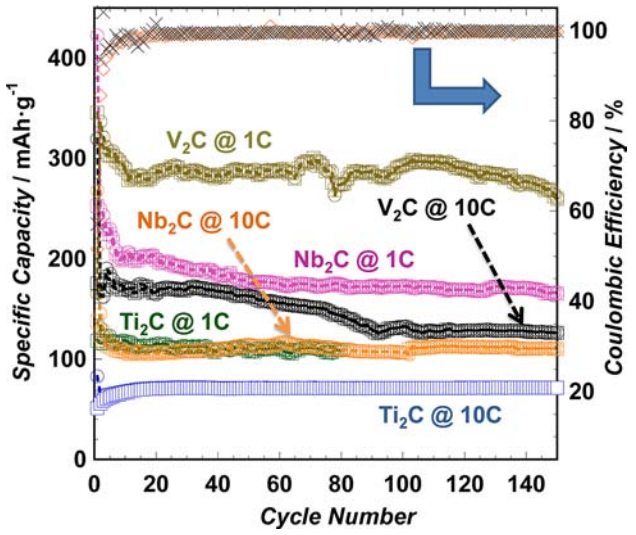

Figure 4. Specific lithiation (circles.) and delithiation (squares) capacities (per mass of active material) vs cycle number at different rates for Nb_2CT_x and V_2CT_x-based electrodes (produced by HF treatment of attrition milled V_2AlC at RT for 8 h) compared to previously reported Ti_2C.[11a]

produced from unmilled V_2AlC. This can be explained by the decreased particle size, facilitating Li diffusion between the layers. A reversible capacity of 288 $mA{\cdot}h{\cdot}g^{-1}$ was obtained instead of 210 $mA{\cdot}h{\cdot}g^{-1}$ at the same cycling rate of 1 C after 50 cycles. A reversible capacity of 260 $mA{\cdot}h{\cdot}g^{-1}$ was obtained for the V_2CT_x, produced by etching attrition milled V_2AlC, after 150 cycles.

More than 2/3 of the reversible lithiation capacity for Nb_2CT_x is below 1 V (Figure 3a), while for both Ti_3C_2[11c] and Ti_2C[11a], the capacities below 1 V were about 1/2 of the reversible capacity. Conversely, in the case of V_2CT_x, less than 1/2 of the reversible lithiation capacity is below 1 V and more than 2/3 of the delithiation capacity is at voltages higher than 1.5 V (Figure 3b). This is an important finding since it shows that each MXene has its own active voltage window. With the variety of possible MXenes chemistries, selection of an optimum MXene for a required voltage window can in principle be achieved. Said otherwise, some MXenes could function better as anodes, while others could, in principle, be used as cathode materials for LIBs.

Figure 4 further shows that both Nb_2CT_x and V_2CT_x (produced by HF treatment of attrition milled V_2AlC powders at RT for 8 h) are capable of handling high cycling rates. At 10 C, capacities of 110 $mA{\cdot}h{\cdot}g^{-1}$ for Nb_2CT_x and 125 $mA{\cdot}h{\cdot}g^{-1}$ for V_2CT_x were obtained after 150 cycles. These values are much higher than what was reported for commercial graphite when

dx.doi.org/10.1021/ja405735d | J. Am. Chem. Soc. 2013, 135, 15966−15969

charged and discharged at 10 C (graphite loses more than 80% of its theoretical capacity at 10 C).[19] Also, these values are ≈50% higher than what we reported previously for Ti_2C at the same rate and closer to the capacities obtained at 1 C.[11a] The high rate capability could be explained by the low Li diffusion barrier in MXenes, similar to what was reported for Ti_3C_2.[11b] The coulombic efficiency at the reversible capacity was about 99.6% for Nb_2CT_x at 10 C. For V_2CT_x, it varied between 98% and 100%.

Although the reversible capacity of MXenes at high cycling rates (*i.e.*, 10 C) is comparable to titania based anodes,[20] the latter have maximum theoretical capacities of the order of 170 mA·h·g^{-1} even at slow scan rates, while V_2CT_x (produced from milled V_2AlC) has a reversible capacity of 260 mA·h·g^{-1} at 1 C.

The results obtained herein were obtained on just synthesized and not well purified compounds and should thus be considered quite preliminary. The higher rate performances, however, are encouraging and suggest that Nb_2CT_x and V_2CT_x can be used as promising electrode materials in LIBs, especially for high power applications. For example, the Li-capacities of additives-free fully delaminated $Ti_3C_2T_x$ electrodes were roughly 4 times those of nondelaminated $Ti_3C_2T_x$.[11c] At this time, we have not succeeded in delaminating Nb_2CT_x or V_2CT_x and used as-produced multilayered powders. Another potential avenue is to strip the MXene surfaces of their functional groups since DFT calculations predict that bare surfaces would have even higher Li uptake those that of functionalized MXenes.[11b] Further improvements in Li uptake can be achieved by optimizing and engineering the electrodes' structures and compositions, and/or by introducing additives as reported for other 2D materials.[21a−c]

In summary, by simply immersing Nb_2AlC and V_2AlC powders into concentrated HF solutions at ambient temperatures, two new MXenes, Nb_2CT_x and V_2CT_x, were successfully synthesized. Since the treatment was carried out in an aqueous HF system, both O (OH) and F terminate the surfaces of as-synthesized 2D flakes. Evidence for physisorbed water between the layers was also found. Testing both Nb_2CT_x and V_2CT_x as electrodes materials in LIBs showed that each has its own voltage profile. It follows that while some MXenes could function better as anodes, others could, in principle, be used as cathode materials for LIBs. Nb_2CT_x showed good reversible capacity (170 mA·h·g^{-1} at 1 C) at lower lithiation voltages. On the other hand, V_2CT_x showed higher capacity (210 mA·h·g^{-1} at 1 C, and 260 mA·h·g^{-1} for V_2CT_x produced from attrition milled V_2AlC) at higher lithiation voltages. Both Nb_2CT_x and V_2CT_x showed excellent capability to handle high cycling rates (10 C), suggesting fast Li diffusion between MXene layers and potential use is high power applications.

■ ASSOCIATED CONTENT

Ⓢ Supporting Information

Materials preparations procedures, characterization techniques, XPS results and analysis, electrochemical cyclic voltammetry. This material is available free of charge via the Internet at http://pubs.acs.org.

■ AUTHOR INFORMATION

Corresponding Authors

gogotsi@drexel.edu
barsoumw@drexel.edu

Notes

The authors declare no competing financial interest.

■ ACKNOWLEDGMENTS

This work was supported by the Assistant Secretary for Energy Efficiency and Renewable Energy, Office of Vehicle Technologies of the U.S. Department of Energy under Contract No. DE-AC02-05CH11231, subcontract No. 6951370, under the Batteries for Advanced Transportation Technologies (BATT) Program. The Linköping Electron Microscopy Laboratory was supported by the Knut and Alice Wallenberg Foundation. Dr. Lars-Åke Näslund (Linköping University) is acknowledged for his help in the XPS measurements, and useful discussions.

■ REFERENCES

(1) Novoselov, K. S.; Geim, A. K.; Morozov, S. V.; Jiang, D.; Zhang, Y.; Dubonos, S. V.; Grigorieva, I. V.; Firsov, A. A. *Science* **2004**, *306*, 666.

(2) Novoselov, K. S.; Jiang, D.; Schedin, F.; Booth, T. J.; Khotkevich, V. V.; Morozov, S. V.; Geim, A. K. *Proc. Natl. Acad. Sci. U.S.A.* **2005**, *102*, 10451.

(3) Jeong, S.; Yoo, D.; Jang, J.-t.; Kim, M.; Cheon, J. *J. Am. Chem. Soc.* **2012**, *134*, 18233.

(4) Ma, R.; Sasaki, T. *Adv. Mater.* **2010**, *22*, 5082.

(5) (a) Naguib, M.; Mashtalir, O.; Carle, J.; Presser, V.; Lu, J.; Hultman, L.; Gogotsi, Y.; Barsoum, M. W. *ACS Nano* **2012**, *6*, 1322. (b) Naguib, M.; Kurtoglu, M.; Presser, V.; Lu, J.; Niu, J.; Heon, M.; Hultman, L.; Gogotsi, Y.; Barsoum, M. W. *Adv. Mater.* **2011**, *23*, 4248.

(6) Barsoum, M. W. *MAX Phases: Properties of Machinable Ternary Carbides and Nitrides*; Wiley VCH GmbH & Co.: Weinheim, Germany, 2013.

(7) (a) Shein, I. R.; Ivanovskii, A. L. *Comput. Mater. Sci.* **2012**, *65*, 104. (b) Khazaei, M.; Arai, M.; Sasaki, T.; Chung, C.-Y.; Venkataramanan, N. S.; Estili, M.; Sakka, Y.; Kawazoe, Y. *Adv. Funct. Mater.* **2012**, *23*, 2185.

(8) Kurtoglu, M.; Naguib, M.; Gogotsi, Y.; Barsoum, M. W. *MRS Commun.* **2012**, *2*, 133.

(9) Zhang, X.; Xu, J.; Wang, H.; Zhang, J.; Yan, H.; Pan, B.; Zhou, J.; Xie, Y. *Angew. Chem., Int. Ed.* **2013**, *52*, 4361.

(10) Lukatskaya, M. R.; Mashtalir, O.; Ren, C. E.; Dall'Agnese, Y.; Rozier, P.; Taberna, P. L.; Naguib, M.; Simon, P.; Barsoum, M. W.; Gogotsi, Y. *Science* **2013**, *341*, 1502.

(11) (a) Naguib, M.; Come, J.; Dyatkin, B.; Presser, V.; Taberna, P.-L.; Simon, P.; Barsoum, M. W.; Gogotsi, Y. *Electrochem. Commun.* **2012**, *16*, 61. (b) Tang, Q.; Zhou, Z.; Shen, P. *J. Am. Chem. Soc.* **2012**, *134*, 16909. (c) Mashtalir, O.; Naguib, M.; Mochalin, V. N.; Dall'Agnese, Y.; Heon, M.; Barsoum, M. W.; Gogotsi, Y. *Nat. Commun.* **2013**, *4*, 1716.

(12) Come, J.; Naguib, M.; Rozier, P.; Barsoum, M. W.; Gogotsi, Y.; Taberna, P.-L.; Morcrette, M.; Simon, P. *J. Electrochem. Soc.* **2012**, *159*, A1368.

(13) Scherrer, P. *Göttinger Nachr. Math. Phys.* **1918**, *2*, 98.

(14) Mashtalir, O.; Naguib, M.; Dyatkin, B.; Gogotsi, Y.; Barsoum, M. W. *Mater. Chem. Phys.* **2013**, *139*, 147.

(15) Crosnier-Lopez, M.-P.; Le Berre, F.; Fourquet, J.-L. *J. Mater. Chem.* **2001**, *11*, 1146.

(16) Viculis, L. M.; Mack, J. J.; Mayer, O. M.; Hahn, H. T.; Kaner, R. B. *J. Mater. Chem.* **2005**, *15*, 974.

(17) Mai, L.; Xu, L.; Hu, B.; Gu, Y. *J. Mater. Res.* **2010**, *25*, 1413.

(18) Sasidharan, M.; Gunawardhana, N.; Yoshio, M.; Nakashima, K. *Mater. Res. Bull.* **2012**, *47*, 2161.

(19) Sivakkumar, S. R.; Nerkar, J. Y.; Pandolfo, A. G. *Electrochim. Acta* **2010**, *55*, 3330.

(20) Yang, Z.; Choi, D.; Kerisit, S.; Rosso, K. M.; Wang, D.; Zhang, J.; Graff, G.; Liu, J. *J. Power Sources* **2009**, *192*, 588.

(21) (a) Su, Y.; Li, S.; Wu, D.; Zhang, F.; Liang, H.; Gao, P.; Cheng, C.; Feng, X. *ACS Nano* **2012**, *6*, 8349. (b) Xiao, J.; Choi, D.; Cosimbescu, L.; Koech, P.; Liu, J.; Lemmon, J. P. *Chem. Mater.* **2010**, *22*, 4522. (c) Lee, J. K.; Smith, K. B.; Hayner, C. M.; Kung, H. H. *Chem. Commun.* **2010**, *46*, 2025.